ACS Catalysis

pubs.acs.org/acscatalysis

Research Article

Correlating the Reverse Water−Gas Shift Reaction with Surface Chemistry: The Influence of Reactant Gas Exposure to Ni(100)

Kyung-Jae Lee, Yifan Ye, Hongyang Su, Bongjin S. Mun,* and Ethan J. Crumlin*

Cite This: *ACS Catal.* 2023, 13, 9041−9050

Read Online

ACCESS | Metrics & More | Article Recommendations | Supporting Information

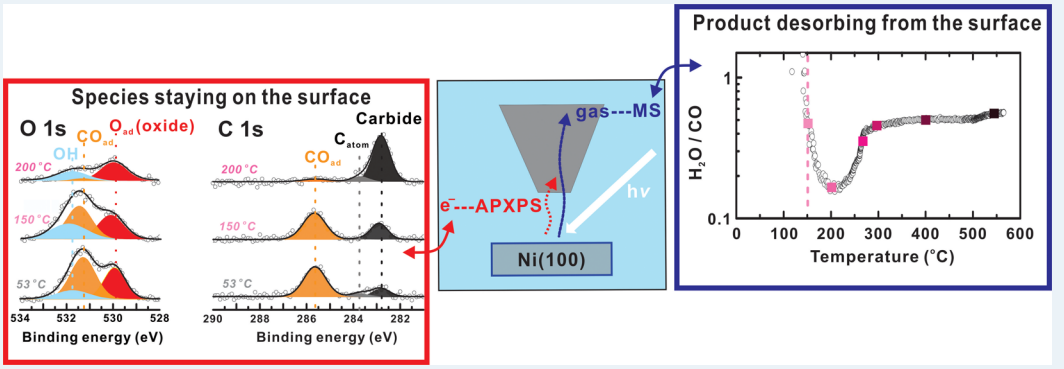

ABSTRACT: Using ambient pressure X-ray photoelectron spectroscopy (APXPS) and mass spectrometry (MS) while varying the temperature, we were able to directly understand how the sequence of exposing reactant gases, CO_2 and H_2, influenced the surface species and reverse water−gas shift reaction product formation on Ni(100). When first dosing CO_2 at room temperature (RT), the Ni(100) surface shows a significant amount of surface oxide due to CO_2 spontaneously dissociating into CO and O and this is nearly unchanged upon introducing H_2. However, when H_2 is dosed first to the nickel surface and CO_2 is subsequently introduced, the spontaneous dissociation of CO_2 still continues yet it forms less surface oxide due to the pre-adsorbed hydrogen on the surface. Interestingly, the major product of CO_2 dissociation from both reactions is a surface oxide, while only a small amount of OH species is observed in either exposure case. This observation confirms that the dominant pathway of CO_2 dissociation on Ni(100) follows the redox mechanism. As the temperature increases, the adsorbed CO further dissociates into atomic carbon and oxygen. As the temperature continues to increase, the influence of the reactant gas exposure sequence no longer exists: the desorption of CO as CO(g) takes place in both cases. It is to note that the surface oxide is present on a nickel surface even at high temperatures over 400 °C, indicating kinetic rate differences between the adsorbed CO desorption and surface oxide hydrogenation to H_2O. Our results reveal how the sequence of dosing gases affects the surface reactivity of the catalyst, providing important insight into the behavior of the catalyst surfaces and their product formation.

KEYWORDS: *ambient pressure X-ray photoelectron spectroscopy, reverse water−gas shift reaction, reaction mechanism, heterogeneous catalysis, CO_2 activation*

1. INTRODUCTION

Repurposing CO_2 has attracted significant attention in many areas, ranging from the concern for climate change to industry utilizing it as an abundant and inexpensive starting material for various valuable chemical processes, including the production of methane, high-order hydrocarbon species, Fischer−Tropsch processes, hydroformylation, and carbonylation.[1−4] CO_2 hydrogenation and the reverse water−gas shift reaction are among many chemical reactions involving CO_2 that have been studied extensively. Due to the inert chemical nature of CO_2, high activation energy barriers inhibit all of these desirable chemical reactions from occurring, necessitating the use of catalysts to promote these chemical reactions. To enhance the performance of these catalysts, fundamental insight that correlates the surface chemistry with the reaction products under operating conditions is needed. Greater insight into the reaction mechanisms between reactants and catalysts will enable the development of efficient catalysts.[5,6]

Nickel is a promising catalyst for dissociating CO_2 to CO with the reverse water−gas shift reaction (RWGS, $CO_2 + H_2 \rightarrow CO + H_2O$). In general, the conversion of CO from CO_2

Received: April 4, 2023
Published: June 23, 2023

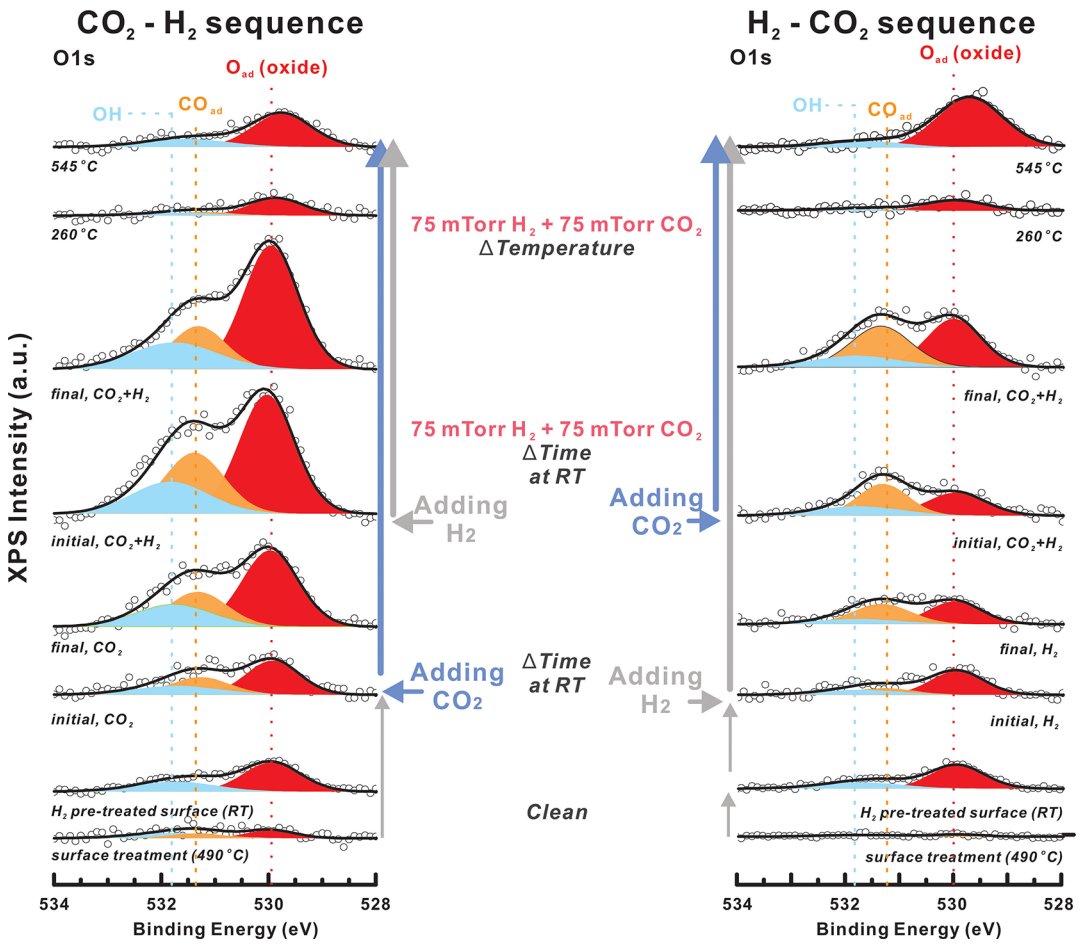

Figure 1. Schematic of the experimental sequences and corresponding O 1s spectra of the initial and final states for each step. The incident photon energy was 690 eV, and the spectra in the figure are displayed without normalization; therefore, the spectra intensities can be directly compared.

with the RWGS reaction is an important step in CO_2 hydrogenation. The RWGS reaction can also serve as an intermediate step in the methanation reaction, followed by the methanation of CO, and is relevant to methanol synthesis from CO_2 via the reverse methanol steam reforming reaction.[7,8] Understanding the RWGS reaction mechanism is therefore crucial for determining the first step of various CO_2 hydrogenation reactions. The two primary reaction mechanisms proposed are the redox mechanism and the hydrogen-mediated mechanism.[9−17] The redox mechanism proposes that CO_2 dissociates directly on the catalyst surface to CO and O, followed by the hydrogenation of O to water.[9,15−17] Weatherbee and Bartholomew confirmed the dissociation of CO_2 into CO and O in the CO_2 hydrogenation reaction with a Nickel/SiO_2 catalyst.[9] Using density functional theory (DFT) calculations, Dietz et al. proposed that the elemental step of the RWGS reaction is determined by the interaction between the catalyst and adsorbed oxygen, and the reaction on nickel will follow the redox mechanism.[16] Alternatively, according to the hydrogen-mediated mechanism, hydrogen first reacts with CO_2 to form carboxyl (COOH) or formate (HCOO), which then dissociates into CO and OH, followed by the hydrogenation of OH to water.[12−14] Vesselli et al. observed hydrogen-assisted CO_2 activation via a carboxyl intermediate on Ni(110) under ultra-high vacuum (UHV) conditions, while Lin et al. found, by using a high-quality Born−Oppenheimer molecular dynamics simulation, that the hydrogen-mediated mechanism is important at low temperatures (90 K).[12,13] The mechanism of the RWGS reaction is still actively debated, and the details, such as the experimental temperature and the gas composition to which the catalyst is exposed, should be considered to identify the mechanism.

To verify the reaction mechanism of the RWGS reaction experimentally, it is important to carefully select the gaseous atmospheres to which a catalyst is exposed. One aspect that needs to be considered is the presence of hydrogen: previous studies have observed a direct dissociation of CO_2 on Ni(111) and Ni(100) in ambient pressure conditions.[18,19] However, the observed direct dissociation does not necessarily imply that the conversion of CO from CO_2 follows the redox mechanism because it cannot exclude the possibility that hydrogen plays a role in the CO_2 activation process. There are also a few examples of hydrogen modifying the surface chemistry of nickel. Subsurface hydrogen, which is more reactive than surface-bound hydrogen, can play an important role in various heterogeneous catalysis processes, such as the hydrogenation of hydrocarbons.[20−22] There is a chance that CO_2 activation could follow a different mechanism if hydrogen co-exists with CO_2. To clarify the mechanism of the RWGS reaction, especially the role of hydrogen, the study of CO_2 activation that involve pre-dosed hydrogen is necessary. The other aspect to consider in the study is the dosing sequence of reactants. Using sum frequency generation spectroscopy, Ghosh et al. found that changing the gas feed ratio and the sequence of

https://doi.org/10.1021/acscatal.3c01517
ACS Catal. 2023, 13, 9041−9050

reactant gases (e.g., H_2 and C_2H_4) could affect competitive adsorption and its resulting intermediates on the catalyst surface.[23] Using a time-resolved analysis of chemical transients during abrupt changes in the reactant partial pressures, Vesselli et al. also showed variations in CO_2 conversion rates with the dosing sequence of gases.[24] Therefore, it is crucial to understand how the dosing sequence of reactants affects the surface of a catalyst and its reactivity by using a well-defined model single crystal surface, which can provide critical insights for utilizing catalysts efficiently.

In this study, using ambient pressure X-ray photoelectron spectroscopy (APXPS) and mass spectrometry (MS), we present results collected simultaneously under two different gas dosing conditions from room temperature (RT) to ∼540 °C on a Ni(100) surface: (1) hydrogen is pumped out after a hydrogen pre-treatment for cleaning the surface is applied. Then, CO_2 is dosed at 75 mTorr followed by 75 mTorr of H_2 (H_2 pre-treated surface $-CO_2$ $-H_2$ sequence), and (2) a total of 75 mTorr of H_2 is maintained after hydrogen pre-treatment. Then, 75 mTorr CO_2 is introduced (H_2 pre-treated surface $-H_2$ $-CO_2$ sequence) (Figure 1). APXPS is a powerful tool for observing the chemical state of surface species under elevated pressures, up to hundreds of mTorr, with various gas conditions, providing direct observations of how the reaction proceeds and what may form during the reaction.[25−27] Our results show that at RT, CO_2 directly dissociates on the hydrogen pre-treated Ni(100) surface to CO and O, supporting the redox mechanism. The resulting atomic oxygen (surface oxide)—the reaction product—can then block Ni(100) surface active sites, resulting in reduced CO_2 conversion rates when CO_2 is dosed first.[24] Correlating surface species, i.e., the CO, atomic carbon, and surface oxide changes during the temperature increase, with MS, we found that the nature of the changes in CO dissociation and CO desorption kinetics aligns with previous theoretical results, and the primary products from the reaction are CO and H_2O.[28] This observation suggests that RWGS is the dominant reaction occurring via the redox reaction mechanism pathway. Furthermore, with quantitative analysis of the CO and H_2O gases, we deduce the origin of the oxide on the Ni(100) surface at high temperatures and relate it to the kinetics of CO and H_2O formation.

2. EXPERIMENTAL SECTION

2.1. Beamline Information and Sample Treatment. Experiments were performed at beamline 9.3.2 of the Advanced Light Source, Lawrence Berkeley National Laboratory. The beamline provides soft X-ray light from a bending magnet in the range of 200−800 eV, and the typical X-ray spot size is 0.5 mm (V) × 1.5 mm (H) with a 15° incident angle. The analyzer system (the R4000 HiPP) consists of a Scienta R4000 with a two-dimensional detector, and the pass energy was set to 100 eV with steps of 100 meV. More detailed information on the specifications of the beamline and end-station can be found elsewhere.[29] Prior to APXPS measurements, the sample surface was treated with several cycles of Ar^+ sputtering (5.0×10^{-6} Torr, 2.0 kV, 20 mA, 45 min) and annealing at UHV (620 °C for 5 min) to achieve an ordered surface. After this cleaning procedure, some residual carbon and oxygen were observed on the surface. To remove these residues and to form the hydrogen pre-treated surface, the sample surface was further treated with 40 mTorr of H_2 at 450 °C. For the use of H_2 gas, a liquid nitrogen trap was installed to avoid any H_2O contamination from the H_2 gas dosing experiment. H_2 was then removed under elevated temperature conditions, returning to UHV conditions before cooling the sample to RT. Survey spectra after H_2 treatment are shown in Figure S1. Following sample treatment, the coverage of impurities such as CO and atomic carbon is estimated at less than 0.1 ML. The (1 × 1) LEED patterns are achieved on the surface at 124 eV (Figure S1). The MS was connected to the second stage of a differential stage behind the front nozzle for residual gas analysis (Ameteck Dycor LC100 residual gas analyzer and quadrupole mass spectrometer).[30]

2.2. Measurement of APXPS Spectra and MS Data. The base pressure of the main chamber was 1.9×10^{-9} Torr, and the pressure of the dosed gas was controlled with a metal leak valve connected to the main chamber (the gases used in the experiment were purchased from PRAXAIR). While introducing gas and waiting for the system to reach an equilibrium state, we collected simultaneously C 1s and O 1s photoemission spectra with a photon energy of 690 eV to monitor how the surface species evolved. After the system reached equilibrium pressure, the photoemission spectra of C 1s, O 1s, Ni 3s, Ni 3p, and the valence band (VB) were measured at a photon energy of 690 eV, and those of C 1s and VB were measured at a photon energy of 440 eV. Photon energies were selected to have similar photoelectron kinetic energies for O 1s and C 1s close to 160 eV to provide similar photoelectron probing depths for the XPS data. During the experiment, MS data were collected simultaneously to monitor reactant and product formation promoted by the surface reaction. By repeatedly comparing spectra at two different positions separated by a distance of 2 mm (Figure S2), we confirmed that no beam damage occurred. All the binding energy positions of the photoemission spectra were calibrated with the Fermi level. O 1s and C 1s spectra were fitted with a combined Gaussian−Lorentzian line shape after subtraction of the Shirley background.

3. RESULTS AND DISCUSSION

3.1. Reaction at RT. *3.1.1. Reaction on the H_2 Pre-Treated Surface: H_2 Pre-Treated Surface $-CO_2$ $-H_2$ Sequence.* First, we introduced 40 mTorr of H_2 and increased the temperature of the sample holder to remove the residuals on Ni(100) and, simultaneously, to create a hydrogen pre-treated surface. While decreasing the temperature after cleaning the catalyst surface, we removed H_2 in the main chamber by opening the gate valve of a turbo molecular pump (TMP) without turning on an ion gauge, which prevented introducing any impurities from the ion gauge.[18] While the pressure of residual H_2 in the main chamber is unknown during this period, we expect, empirically, that the pressure of H_2 in the main chamber should be below 10^{-8} Torr upon opening the TMP gate valve. According to a previous study on H_2 adsorption behavior and kinetics on Ni(100) with adsorption isotherm and laser induced thermal desorption techniques,[31−33] H_2 dissociates over the topmost nickel atom and adsorbs on either hollow sites or bridge sites.[32] Panczyk et al. studied how the H_2 coverage changes with temperature and H_2 pressure: H_2 coverage on Ni(100) is approximately 0.65 ML at 41 °C and 1×10^{-8} Torr of H_2 and it reaches saturation coverage, 0.86 ML at 3×10^{-7} Torr of H_2.[32] Although the coverage of H_2 on Ni(100) after the H_2 pre-treatment is unknown, due to a lack of information and the limitations on measuring hydrogen with XPS, it is estimated that the coverage

https://doi.org/10.1021/acscatal.3c01517
ACS Catal. 2023, 13, 9041−9050

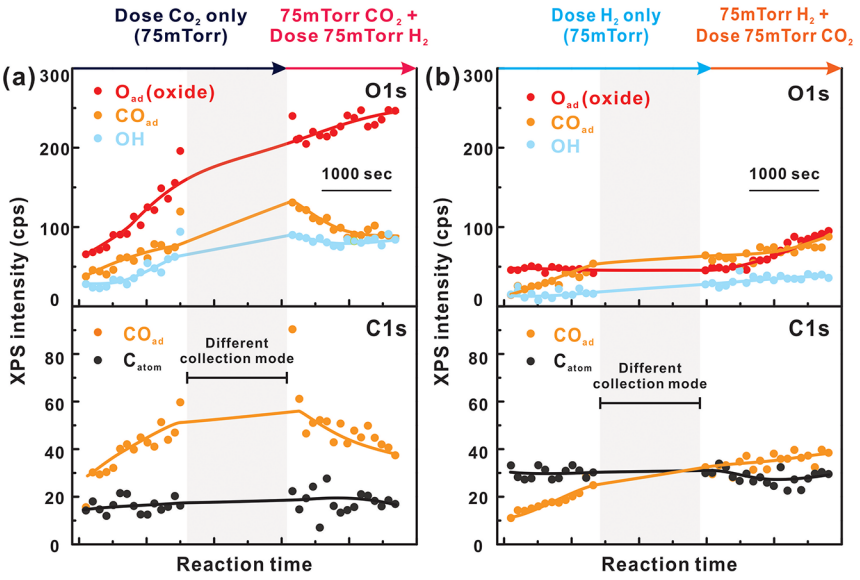

Figure 2. APXPS measurement of the surface species on Ni(100) over time as the gas composition changes at RT. (a) H_2 pre-treated surface $-CO_2$ $-H_2$ sequence and (b) H_2 pre-treated surface $-H_2$ $-CO_2$ sequence. During the different collection mode regions (gray region in the figure), O 1s, C 1s, Ni 3s, Ni 3p, and valence band spectra with different photon energies and higher iteration numbers were measured. The experiment time is reflected in the figure.

of H_2 on Ni(100) after H_2 pre-treatment is less than its saturation coverage. This hydrogen pre-treated surface with sites for CO_2 adsorption is an appropriate environment to investigate the role of H_2 on CO_2 activation.

After H_2 pre-treatment, 75 mTorr of CO_2(g) was dosed into the main chamber at RT, and C 1s, O 1s, and VB spectra were collected with 690 eV incident photon energy (Figures 1, S3, and S4). Under 75 mTorr of CO_2, the peaks at 285.7 eV in the C 1s spectrum and 531.3 eV in the O 1s spectrum correspond to adsorbed CO (CO_{ad}), while the peak at 530.0 eV in the O 1s spectrum is surface oxide (O_{ad}) (Table S1). Both CO_{ad} and O_{ad} peaks increase gradually with time (Figure 2a), indicating that CO_2 dissociates into CO_{ad} and O_{ad} on the hydrogen pre-treated Ni(100) surface. Small amounts of O_{ad} and OH_{ad} exist on the surface just after dosing CO_2, which come from impurities in the chamber and from remaining H_2 after hydrogen pre-treatment. When reaching equilibrium after CO_2 dosing, there is an increase in the amount of OH_{ad} but the dominant increased species is O_{ad}. This result suggests that the dominant pathway of CO_2 activation follows the redox mechanism even when hydrogen is on the surface. Otherwise, according to the hydrogen mediated mechanism, the major products would be CO_{ad} and OH_{ad} at 531.8 eV in the O 1s spectra (Table S1).

After reaching equilibrium with 75 mTorr of CO_2, no carbonate, 288.9 eV in the C 1s spectra, was observed. On the contrary, carbonate was seen under UHV conditions on Ni(100) and near ambient pressure conditions on Ni(111) (Table S1).[18,34] Previous studies demonstrated that pre-adsorbed oxygen on a nickel surface reacts with CO_2 to form carbonate. The absence of carbonate at near ambient pressure on Ni(100) was reported in a previous CO_2 activation study on Ni(111) and Ni(100).[19] With DFT calculations, the authors found that the adsorption of CO_2 on Ni(100) is strong and the subsequent dissociation of CO_2 is much easier than that on Ni(111), leading to less favorable carbonate formation on Ni(100). This explanation is consistent with our experimental results, which informs us that carbonate is not the intermediate in the case of CO_2 activation with H_2 on Ni(100).

There are peaks at 282.9 and 283.8 eV corresponding to carbidic and graphitic carbon, respectively, which are common carbon species on nickel surfaces (Table S1)[35,36] Rodriguez et al. investigated the catalytic properties of metal carbides and the interaction between metal carbides and a supported metal.[4] However, it has been reported that metallic nickel catalysts are more active than nickel carbide for dry reforming reaction that utilizes CO_2.[37] In addition, there was no direct evidence that this small amount of carbidic carbon exerted a specific role in the reaction with CO_2. A small amount of graphitic and carbidic carbon visible in the first C 1s spectrum (Figure S4) was designated as "atomic carbon (C_{atom})." As the hydrogen pre-treated Ni(100) surface is exposed to 75 mTorr CO_2 as a function of time, there is no apparent change in the amount of C_{atom} (Figure 2a), indicating that no further reaction occurs to produce atomic carbon from CO_{ad} (CO_{ad} dissociation) at RT. According to a previous study, the activation barrier for CO dissociation on Ni(100) is >1.2 eV.[38] Thus, even considering the hydrogen-assisted route, CO dissociation at RT is not plausible.

After equilibrating with 75 mTorr of CO_2, 75 mTorr of H_2(g) was added at RT, and the changes in surface species were examined (Figures 2a and S4). The CO_{ad} peaks at 285.7 eV in the C 1s spectra and 531.3 eV in the O 1s spectra decrease as a function of time, while the population of other species remains largely unchanged. If the addition of H_2 assisted CO_2 activation on the Ni(100) surface, we would see an increase in the product of CO_2 dissociation, CO_{ad}, and the oxygen component, such as O_{ad} or OH_{ad}. However, the decrease in CO_{ad} reflects that added H_2 did not promote the reactions. We rationalize this observation by noting that the reaction sites for CO_2 dissociation had already been covered with surface species (e.g., CO_{ad}, O_{ad}, and H_{ad}) and conclude that competitive adsorption between H_2 and CO_{ad} on the nickel surface would decrease the amount of CO_{ad}.[39,40]

https://doi.org/10.1021/acscatal.3c01517
ACS Catal. 2023, 13, 9041−9050

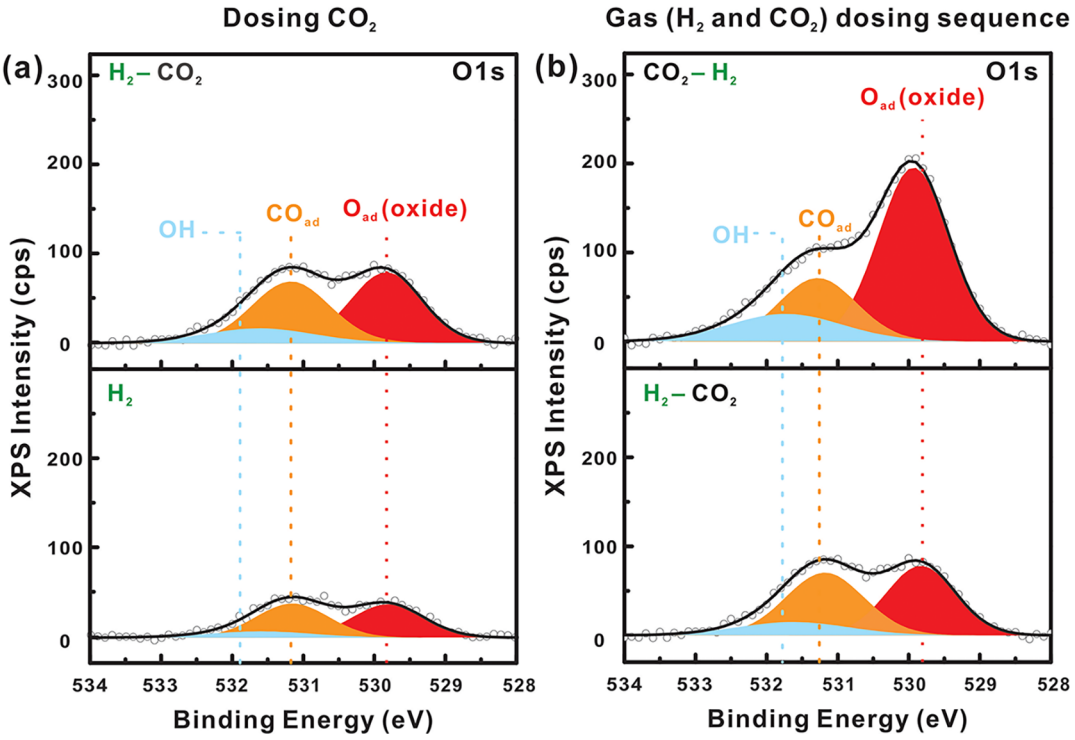

Figure 3. Different chemical states after reaching equilibrium at room temperature. (a) O1s spectra after equilibrium in a H_2 atmosphere only (H_2 pre-treated surface $-H_2$, lower) and in a H_2 + CO_2 atmosphere (H_2 pre-treated surface $-H_2$ $-CO_2$, upper). (b) O1s spectra after equilibrium in two different sequences of dosing gases: H_2 pre-treated surface $-H_2$ $-CO_2$ sequence (lower), H_2 pre-treated surface $-CO_2$ $-H_2$ sequence (upper).

3.1.2. Reaction in the H_2 Pre-Dosed Case: H_2 Pre-Treated Surface $-H_2$ $-CO_2$ Sequence. To understand the effect of changing the sequence of dosing gases and the influence of increased hydrogen surface coverage on CO_2 activation, we exposed hydrogen pre-treated Ni(100) to 75 mTorr of H_2(g) at RT. According to previous research, hydrogen coverage on Ni(100) reaches its saturation value, 0.858, at 3×10^{-7} Torr of H_2.[32] Therefore, the hydrogen coverage in this H_2 pre-dosed case, i.e., 75 mTorr of H_2, should be saturated. Under the H_2 pre-dosed condition, CO_{ad} increased slightly as a function of time, as observed from changes in the C 1s and O 1s spectra (Figures S5 and 2b). Since CO_2 gas had not yet been introduced, we believe that the increase in CO_{ad} originated from residual CO in the main chamber despite reaching UHV base pressures of low 10^{-9} Torr.[41] While a spectral signature of hydrogen adsorption is difficult to observe directly with XPS, it is expected that in the H_2 pre-dosed condition, the nickel surface is composed of bare nickel metal covered primarily with H_{ad} and small amounts of CO_{ad}, C_{atom}, O_{ad}, and OH_{ad}.

As 75 mTorr of CO_2(g) is added to the H_2 pre-dosed environment, CO_{ad} increases but to a lesser extent compared with first dosing CO_2 under H_2 pre-treated conditions. Quantifying from the O 1s spectra, there was 82% more CO_{ads} when CO_2 was dosed first in the H_2 pre-treated condition as opposed to dosing H_2 followed by CO_2. The smaller increase in CO_{ad} in the case of dosing H_2 first (H_2 pre-dosed condition) is attributed to the high H_{ad} surface coverage on Ni(100) blocking the adsorption of CO_2. According to previous DFT calculations, dissociated CO_{ad} and O_{ad} prefer to chemisorb on hollow sites on Ni(100).[42] As mentioned above, when H_2 is dosed first, dissociated H_{ad} adsorbing on hollow sites or bridge sites of the Ni(100) surface could prohibit CO_2 from dissociating into CO_{ad} and O_{ad}, resulting in a small increase in CO_{ad}. The peak maxima in hydrogen desorption experiments on Ni(100) appear at approximately 350 K (ca. 75 °C), thus reinforcing the hypothesis that at RT, H_{ad} blocks the adsorption sites for the products of CO_2 dissociation.[43] In contrast, in the spectra before and after dosing 75 mTorr of CO_2 under H_2 pre-dosed conditions, the increases in CO_{ad} and O_{ad} were dominant (Figure 3a). This result indicates that regardless of the hydrogen coverage, CO_2 dissociates directly into CO_{ad} and O_{ad} with H_2 on Ni(100) at RT.[18] If the dominant pathway of CO_2 activation with H_2 follows the hydrogen-mediated mechanism, carboxyl (or formate) would dissociate into CO_{ad} and OH_{ad} and there would be an increase in OH_{ad}, rather than O_{ad}, species. If carboxyl (or formate) has not yet dissociated, formate (or carboxyl) should be observed at 288.0 eV in the C 1s spectra, but there is no peak in this region (Figures S3 and S4).[14] Therefore, the increase in O_{ad} with CO_{ad} in the O 1s spectra supports the conclusion that the dominant reaction route of CO_2 activation on Ni(100) with H_2 follows the redox mechanism. This finding is further supported by Dietz et al., who reported a systematic DFT analysis of the RWGS reaction in which metals with high affinity toward oxygen, such as Rh, Ni, and Cu, prefer CO_2 activation via the CO_2 dissociation pathway ($CO_2 \rightarrow CO_{ad} + O_{ad}$), while for metals with weak affinity toward oxygen, such as Pt, Ag, and Pd, hydrogen is involved in CO_2 activation via carboxyl or formate formation.[16] The affinity of the catalyst to oxygen, which strongly affects the dissociation activation energy, is the main parameter determining the dominant reaction pathway.

Regardless of the CO_2 dosing conditions, i.e., H_2 pre-treated and pre-dosed conditions, the surface species are the same, but the amount of O_{ad} surface coverage is different (Figure 3b). This observation implies that the surface species coverage can vary according to the order in which gases are exposed to a

https://doi.org/10.1021/acscatal.3c01517
ACS Catal. 2023, 13, 9041−9050

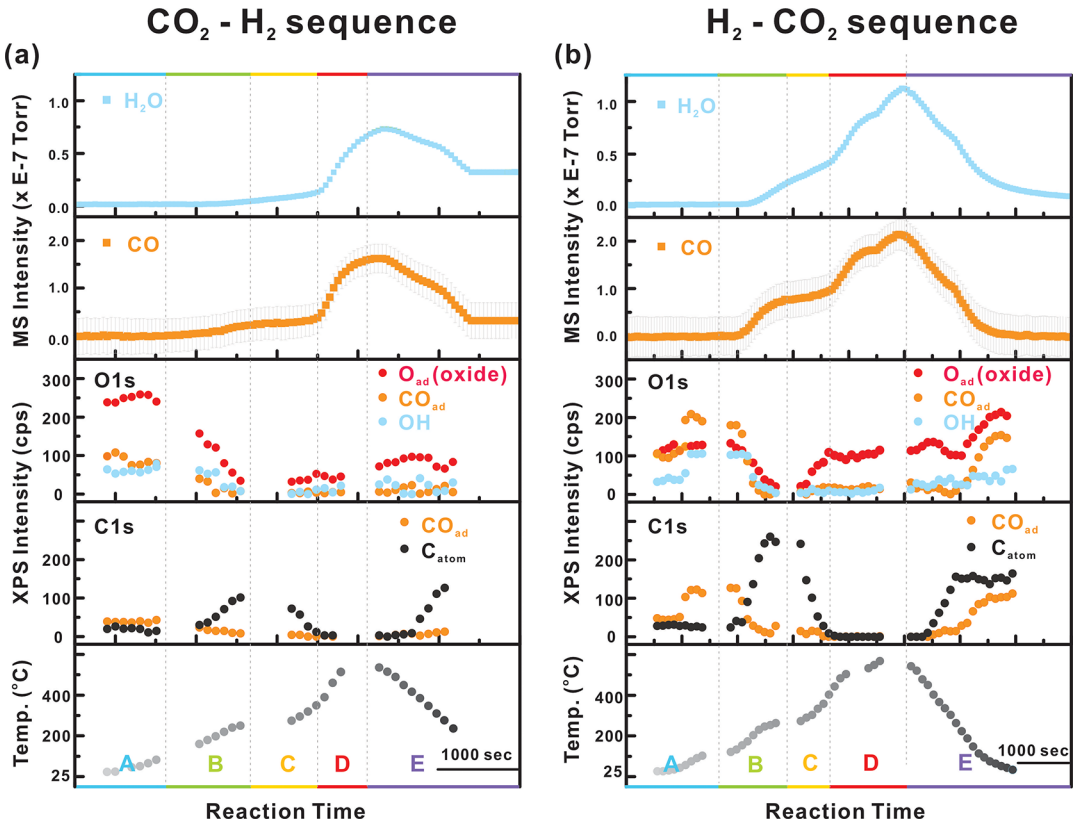

Figure 4. APXPS of the surface species and mass spectrometer measurement of the product on Ni(100) as the temperature changes. (a) H_2 pre-treated surface $-CO_2$ $-H_2$ sequence and (b) H_2 pre-treated surface $-H_2$ $-CO_2$ sequence (the data treatment of the mass spectrometer is explained in Figure S8).

catalyst surface, even when the final gas composition is identical. Vesselli et al. reported that the CO_2 methanation conversion ratio in the early phase for the case of dosing CO_2 first and adding H_2 later is much smaller than the opposite sequence.[24] They claimed that the conversion ratio could be affected by the presence of hydrogen and by co-adsorption effects. However, based on our experiments, H_2 is not involved in CO_2 activation, which is the first step in CO_2 methanation on Ni(100). Instead of a H_2 effect, this result might be explained by the O_{ad} coverage effect: when CO_2 is dosed first, it dissociates into CO_{ad} and O_{ad}, and O_{ad} could cover a large portion of the nickel surface, deactivating the catalyst surface and giving rise to the reduced conversion ratio.

3.2. Reaction at Elevated Temperatures. *3.2.1. Reaction on the H_2 Pre-Treated Surface: H_2 Pre-Treated Surface $-CO_2$ $-H_2$ Sequence.* After reaching the equilibrium state with 75 mTorr of both CO_2 and H_2 at RT, we observed a change in the surface species of the C 1s and O 1s spectra, along with changing temperature. The formation of the expected products, CO(g) and H_2O(g), was monitored simultaneously with the mass spectrometer (Figures S6 and 4a). In Figure 4a region A, where the temperature is below 108 °C, there are no discernable changes in the XPS intensities of C 1s and O 1s spectra or the mass intensities of CO and H_2O, indicating that the equilibrium state at RT is maintained in this temperature region. As the temperature is further increased above 160 °C, CO_{ad} at 285.7 eV in the C 1s spectrum and O_{ad} at 530.0 eV in the O 1s spectrum begin to decrease, while C_{atom} in the C 1s spectrum increases (Figure 4a, region B). Under these conditions, high temperature with H_2, O_{ad} could be reduced to H_2O, exposing the uncovered sites for further CO_2 activation. In addition, the decrease in CO_{ad} and the increase in C_{atom} reflect that CO_{ad} is dissociated into C_{ad} ($CO_{ad} \rightarrow C_{ad} + O_{ad}$) or goes through a disproportionation reaction ($2CO_{ad} \rightarrow C_{ad} + CO_2(g)$).[38] This trend, therefore, implies that CO_{ad} is an intermediate state for C_{ad}, which is in line with previous studies.[35] In addition, the increase in CO and H_2O in the mass spectrometer supports continuous CO_2 activation under these conditions.

When the temperature increases over 250 °C in Figure 4a region C, there is a decrease in C_{atom} in the C 1s spectra. Meanwhile, the formation of CO and H_2O in the mass spectrometer is measured continuously. C_{atom} is an ingredient for methane, and C_{atom} reacts with H_2 to form methane.[35] Contrary to expectations, however, CH_3, which should be measurable in the presence of methane, is not detected in the mass spectrometer (Figure S10). It may be that the low molar ratio of H_2 in this experiment (CO_2:H_2 = 1:1) gives rise to fewer opportunities for C_{atom} to react with H_2 or that C_{atom} reacts with CO_2 to form CO ($CO_2 + C_{atom} \rightarrow 2CO_{ad} \rightarrow 2CO(g)$).[44]

At temperatures over 390 °C (Figure 4a region D), a clean surface with a small amount of O_{ad} is formed, along with a considerable amount of CO and H_2O, which indicates that RWGS is the major chemical reaction under these conditions. CO_2 methanation and the RWGS reaction are competitive, but the RWGS reaction is favored at high temperatures, and our experimental gas ratio (CO_2:H_2 = 1:1) also favors the RWGS reaction.[45,46] The presence of O_{ad} on the nickel surface in this reductive condition will be discussed later.

With decreasing temperature, (Figure 4a region E) C_{atom} increases in the C 1s spectra and the intensities of CO and

https://doi.org/10.1021/acscatal.3c01517
ACS Catal. 2023, 13, 9041−9050

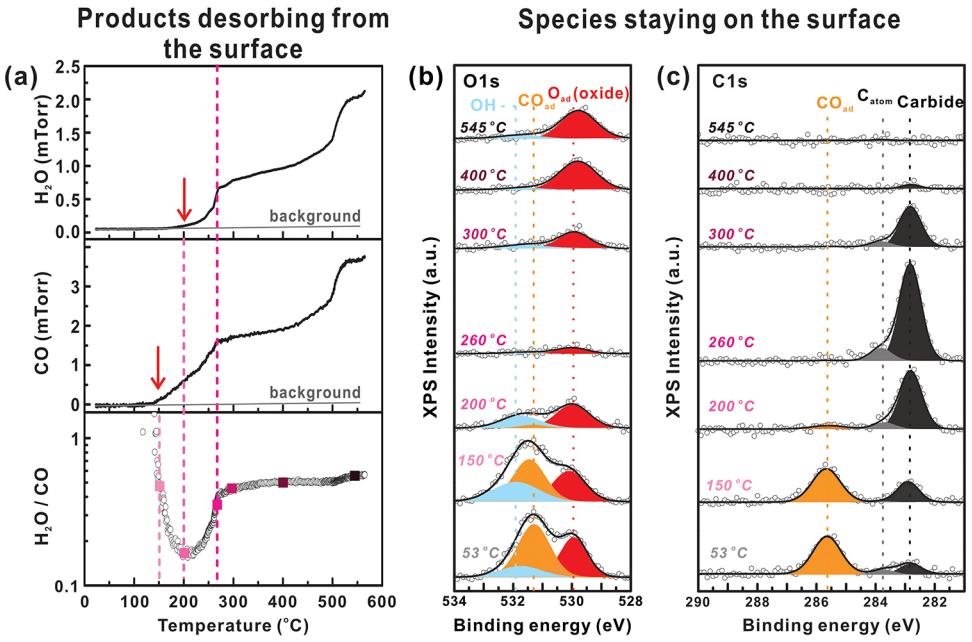

Figure 5. Relation between the surface species and products for the H_2 pre-treated surface $-H_2$ $-CO_2$ sequence. (a) Calibrated CO and H_2O in the main chamber and the ratio between H_2O and CO. Red arrows indicate the onset of CO and H_2O. (b) O 1s and (c) C 1s spectra at the specific temperature. The relation between the surface species and products for the CO_2 $-H_2$ sequence is shown in Figure S11.

H_2O in the mass spectra decrease. At high temperatures, the desorption of CO_{ad} ($CO_{ad} \rightarrow CO(g)$) and the dissociation of CO_{ad} ($CO_{ad} \rightarrow C_{ad} + O_{ad}$) compete against each other, and decreasing the temperature favors the dissociation of CO_{ad} over the desorption of CO_{ad}, resulting in an increase in atomic carbon on the nickel surface. The enhanced surface atomic carbon leads to a decrease in available sites for CO_2 activation, and the reduced kinetics due to decreasing temperature leads to decreases in CO and H_2O in the mass spectra. Note that the reverse sequence in the cooling process reflects the reversibility of this reaction on Ni(100).

3.2.2. Reaction in the H_2 Pre-Dosed Case: H_2 Pre-Treated Surface $-H_2$ $-CO_2$ Sequence. Figures S7 and 4b show C 1s and O 1s spectra, the trends of surface species, and corresponding mass spectra for CO and H_2O along the temperature. Unlike the case for the H_2 pre-treated surface $-CO_2$ $-H_2$ sequence, the peak of CO_{ad} and the peak of OH_{ad} increase (Figure 4b region A) with increasing temperature up to 60 °C. Previous studies have reported that hydrogen desorption could occur as the temperature was raised above RT.[43] Therefore, as the temperature increases, H_{ad} desorbs, exposing new sites for CO_2 dissociation and leading to an increase in surface CO_{ad} and O_{ad}. In addition, further reaction with O_{ad} and hydrogen results in OH_{ad} formation at temperatures higher than RT. On the other hand, in the case of the H_2 pre-treated surface $-CO_2$ $-H_2$ sequence, a large portion of the surface has already been covered with O_{ad}, rather than H_{ad}; thus, the increasing temperature did not create new sites for further CO_2 dissociation.

As the temperature increases further, CO_{ad} and O_{ad} decrease simultaneously. Meanwhile, C_{atom} in the C 1s spectra increases, exhibiting a trend similar to that of the H_2 pre-treated surface $-CO_2$ $-H_2$ sequence (Figure 4b region B). In addition, the formation of CO and H_2O is detected using the mass spectrometer. This trend reveals that reactions in this temperature region do not depend on the dosing sequence of gases. Importantly, three different reactions occur simultaneously in this temperature region: (1) CO_2 dissociation ($CO_2 \rightarrow CO_{ad} + O_{ad}$), (2) CO_{ad} dissociation ($CO_{ad} \rightarrow C_{ad} + O_{ad}$), and (3) CO_{ad} desorption ($CO_{ad} \rightarrow CO(g)$). Based on the fact that increased temperature enhances C_{atom} levels, reaction 2 (CO_{ad} dissociation) appears to dominate in this temperature region. At temperatures between 260 and 400 °C (Figure 4b region C), we see a decrease in C_{atom} in the C 1s spectra, and CO and H_2O formation are continuously detected in the mass spectra similar to the case of H_2 pre-treated surface $-CO_2$ $-H_2$ sequence. In this temperature region, the desorption of CO_{ad} to CO(g), reaction 3, is more favorable than CO_{ad} dissociation, and the existing C_{atom} is oxidized to CO(g), resulting in a continuous decrease in carbon species and detection of CO by the mass spectrometer. In Figure S10, no CH_3 was detected in the mass spectra, just as for the H_2 pre-treated surface $-CO_2$ $-H_2$ sequence, which reflects that methane is not a reaction product. This result is due to the slow kinetics for producing methane and to the experimental conditions of high temperature and high CO_2/H_2 ratio.[45] In addition, O_{ad} starts to increase in this reductive condition.

When the temperature increases further, over 400 °C, C_{atom} disappears from the C 1s spectra, and larger amounts of CO and H_2O are detected using the mass spectrometer, which means that the RWGS reaction dominates under these conditions (Figure 4b region D). When the temperature decreases from 400 °C, C_{atom} in C 1s starts to increase first; as the temperature decreases further, CO_{ad} reappears on the nickel surface, which is the reverse phenomenon of the case of increasing temperature (Figure 4b region E). Again, we see the same trend with the case of dosing CO_2 first and adding H_2 later, which supports the reversibility of this chemical reaction.

To investigate the kinetics of the RWGS reaction at high temperatures, the amounts of CO and H_2O measured in the mass spectrometer were calibrated into the pressure in the main chamber (the correlation between the main chamber pressure and the signal intensity in the mass spectrometer for CO and H_2O appears in Figure S9). In Figure 5, the onset of

https://doi.org/10.1021/acscatal.3c01517
ACS Catal. 2023, 13, 9041−9050

Scheme 1. Scheme of the CO_2 Adsorption and Dissociation on the Ni (100) Surface at Room Temperature and Its Further Conversion at Elevated Temperatures

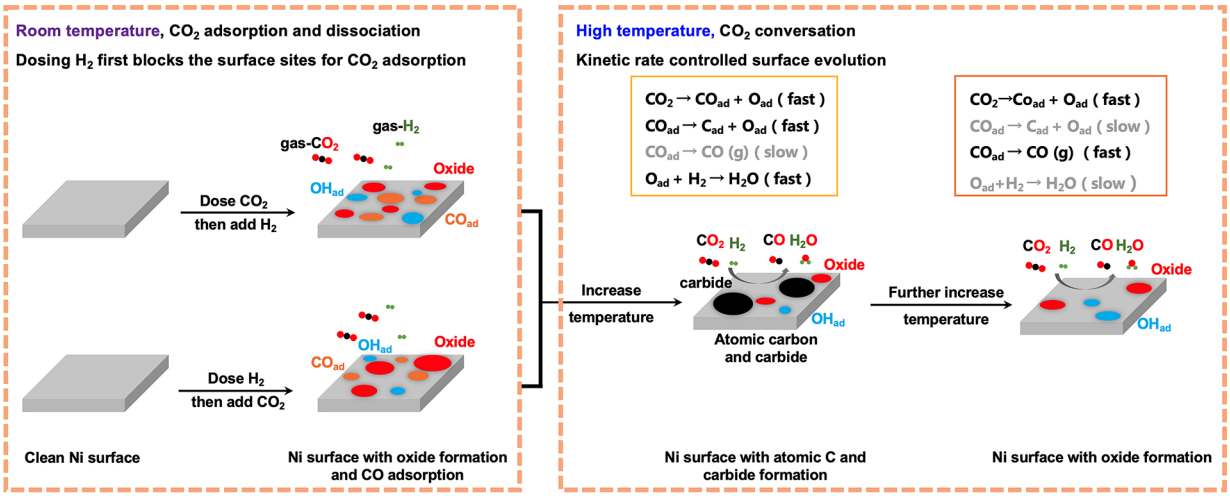

CO detected using the mass spectrometer appears at approximately 150 °C, and the C 1s and O 1s spectra from 150 to 200 °C show that CO_{ad} decreases dominantly. Previous work using temperature programmed desorption (TPD) experiments reported CO desorption on Ni(100) at approximately 150 °C, consistent with the result in this experiment.[43] On the other hand, the onset of H_2O in the mass spectra occurs at approximately 200 °C, and the O 1s spectra from 200 to 260 °C show a decrease in O_{ad}. In addition, the ratio between H_2O and CO is always below 1 in the high-temperature region, which means that the pressure of CO is higher than that of H_2O in the region where the RWGS reaction is dominant. This finding could reflect different kinetics for CO and H_2O: after CO_2(g) dissociates into CO_{ad} and O_{ad} on Ni(100), CO_{ad} is favored to desorb in this high-temperature region. However, to form H_2O(g), O_{ad} needs to react with two H_{ad} and desorb, resulting in slower kinetics than those of CO desorption. This would also be the origin of O_{ad} in the O 1s spectra in this reductive atmosphere (these trends are similar regardless of the dosing sequence of gases, and the result for the case of dosing CO_2 first and adding H_2 later is given in Figure S11).

Finally, the series of changes with temperature for the surface species mentioned above reflects that RWGS reactions on the Ni(100) surface proceed in competition with three primary chemical reactions (Scheme 1): (1) CO_2 dissociation, (2) CO_{ad} dissociation, and (3) CO_{ad} desorption. At low temperatures, the major reaction is CO_2 dissociation into CO_{ad} and O_{ad} via the redox mechanism. As the temperature increases, CO_{ad} dissociation to C_{ad} and O_{ad} starts to occur and CO_{ad} desorption to CO(g) becomes favorable at even higher temperatures.[28] Although the dosing sequence of gases could affect the initial surface coverages of each surface species, especially O_{ad}, it does not change the consequent reactions, which occur via the same processes. In terms of product selectivity, methane or CO, this could be critically influenced by the reaction conditions, such as temperature and molar ratio (or pressure) of reactant H_2. For CO_2 methanation, C_{atom} is a vital intermediate; thus, the CO_{ad} dissociation reaction must be favored to increase the selectivity of methane. At high temperatures, however, CO_{ad} desorption is favored over CO_{ad} dissociation; therefore, a proper and moderate temperature range should be chosen for methanation. To the end, to improve the selectivity of methane, a larger molar ratio of H_2 or a higher pressure of H_2 should be applied to increase the likelihood that C_{ad} and H_{ad} will meet frequently. This work aids in bridging fundamental scientific questions to applied systems providing novel insight into nickel catalysts that are often used in industrial catalysts, which are usually Ni particles supported on silica, alumina, or other reducible metal oxides which will be investigated in future studies.

4. CONCLUSIONS

A detailed investigation of the RWGS reaction on Ni(100) is carried out under a CO_2 + H_2 environment. At RT, CO_2 dissociates into CO_{ad} and O_{ad} in the presence of H_2 on Ni(100). When CO_2 dissociates through the hydrogen-mediated mechanism, its products are CO_{ad} and OH_{ad}. The existence of O_{ad}, rather than OH_{ad}, in our results confirms that CO_2 dissociates with a dominant redox mechanism. In addition, when CO_2 is dosed first, there is more CO_2 dissociation than when H_2 is pre-dosed, due to site blocking by H_{ad} on nickel, resulting in more O_{ad} on nickel with CO_2 dosed first. This larger amount of O_{ad} could hinder further reaction steps; this effect is consistent with the decreased CO_2 conversion rate in the previous report when CO_2 was dosed first.[20]

The surface under H_2 pre-dosed conditions shows an increase in CO_{ad} and O_{ad} with increasing temperature due to the exposure of new active sites for CO_2 dissociation as hydrogen desorbs, and the following trends are similar to the case of the H_2 pre-treated surface $-CO_2$ $-H_2$ sequence. As the temperature increases, CO_{ad} dissociates into C_{atom} and O_{ad}, followed by the hydrogenation of O_{ad} into H_2O. Upon further elevated temperatures, C_{atom} disappears, while O_{ad} is simultaneously observed with CO and H_2O in the mass spectra. These CO behaviors follow the thermodynamic preference: at moderate temperatures, CO_{ad} dissociation is preferred over CO_{ad} desorption, but at high temperatures, CO_{ad} desorption is the most prevalent. In addition, at high temperatures, larger amounts of CO than H_2O are observed in the mass spectra, which is due to the faster kinetics of desorption for CO_{ad} than for the hydrogenation of O_{ad} to H_2O.

https://doi.org/10.1021/acscatal.3c01517
ACS Catal. 2023, 13, 9041−9050

These results are consistent with the O_{ad} observed on nickel surfaces in this high-temperature regime.

■ ASSOCIATED CONTENT

Supporting Information

The Supporting Information is available free of charge at https://pubs.acs.org/doi/10.1021/acscatal.3c01517.

The detailed XPS spectra in AP-XPS measurement, the method of MS intensity calibration for CO and H_2O in the main chamber, and the MS of methane (PDF)

■ AUTHOR INFORMATION

Corresponding Authors

Bongjin S. Mun − *Department of Physics and Photon Science, Gwangju Institute of Science and Technology (GIST), Gwangju 500-712, South Korea;* orcid.org/0000-0002-8525-3298; Email: bsmun@gist.ac.kr

Ethan J. Crumlin − *Advanced Light Source and Chemical Sciences Division, Lawrence Berkeley National Laboratory, Berkeley, California 94720, United States;* orcid.org/0000-0003-3132-190X; Email: ejcrumlin@lbl.gov

Authors

Kyung-Jae Lee − *Advanced Light Source, Lawrence Berkeley National Laboratory, Berkeley, California 94720, United States; Department of Physics and Photon Science, Gwangju Institute of Science and Technology (GIST), Gwangju 500-712, South Korea*

Yifan Ye − *Advanced Light Source, Joint Center for Artificial Photosynthesis, and Chemical Sciences Division, Lawrence Berkeley National Laboratory, Berkeley, California 94720, United States; National Synchrotron Radiation Laboratory, University of Science and Technology of China, Hefei, Anhui 230026, P. R. China*

Hongyang Su − *Advanced Light Source, Lawrence Berkeley National Laboratory, Berkeley, California 94720, United States; Hefei National Laboratory for Physical Science at the Microscale, University of Science and Technology of China, Hefei, Anhui 230026, P. R. China*

Complete contact information is available at: https://pubs.acs.org/10.1021/acscatal.3c01517

Author Contributions

The manuscript was written through contributions of all authors. All authors have given approval to the final version of the manuscript.

Notes

The authors declare no competing financial interest.

■ ACKNOWLEDGMENTS

This research used resources of the Advanced Light Source, which is a DOE Office of Science User Facility under Contract No. DE-AC02-05CH11231. In addition, Y.Y. and E.J.C. were partially supported by an Early Career Award in the Condensed Phase and Interfacial Molecular Science Program, in the Chemical Sciences Geosciences and Biosciences Division of the Office of Basic Energy Sciences of the U.S. Department of Energy under Contract No. DE-AC02-05CH11231. Y.Y. also acknowledges the support from National Natural Science Foundation of China (22172153) and Users with Excellence Program of Hefei Science Center CAS (2021HSC-UE001). Financial support was also provided by the National Research Foundation of Korea (NRF-2020K1A3A7A09080400 and NRF-2022R1A2C2008448) and the GIST Research Institute Grant funded by the GIST 2023.

■ REFERENCES

(1) Nielsen, D. U.; Hu, X.-M.; Daasbjerg, K.; Skrydstrup, T. Chemically and electrochemically catalysed conversion of CO_2 to CO with follow-up utilization to value-added chemicals. *Nat. Catal.* **2018**, *1*, 244−254.

(2) Ma, J.; Sun, N.; Zhang, X.; Zhao, N.; Xiao, F.; Wei, W.; Sun, Y. A short review of catalysis for CO_2 conversion. *Catal. Today* **2009**, *148*, 221−231.

(3) Kattel, S.; Ramírez, P. J.; Chen, J. G.; Rodriguez, J. A.; Liu, P. Active sites for CO_2 hydrogenation to methanol on Cu/ZnO catalysts. *Science* **2017**, *355*, 1296−1299.

(4) Rodriguez, J. A.; Liu, P.; Stacchiola, D. J.; Senanayake, S. D.; White, M. G.; Chen, J. G. Hydrogenation of CO_2 to Methanol: Importance of Metal−Oxide and Metal−Carbide Interfaces in the Activation of CO_2. *ACS Catal.* **2015**, *5*, 6696−6706.

(5) Cheng, D.; Negreiros, F. R.; Aprà, E.; Fortunelli, A. Computational Approaches to the Chemical Conversion of Carbon Dioxide. *ChemSusChem* **2013**, *6*, 944−965.

(6) Wang, W.; Wang, S.; Ma, X.; Gong, J. Recent advances in catalytic hydrogenation of carbon dioxide. *Chem. Soc. Rev.* **2011**, *40*, 3703−3727.

(7) Roiaz, M.; Monachino, E.; Dri, C.; Greiner, M.; Knop-Gericke, A.; Schlögl, R.; Comelli, G.; Vesselli, E. Reverse Water−Gas Shift or Sabatier Methanation on Ni(110)? Stable Surface Species at Near-Ambient Pressure. *J. Am. Chem. Soc.* **2016**, *138*, 4146−4154.

(8) Wu, H. C.; Chang, Y. C.; Wu, J. H.; Lin, J. H.; Lin, I. K.; Chen, C. S. Methanation of CO_2 and reverse water gas shift reactions on Ni/SiO_2 catalysts: the influence of particle size on selectivity and reaction pathway. *Catal. Sci. Technol.* **2015**, *5*, 4154−4163.

(9) Weatherbee, G. D.; Bartholomew, C. H. Hydrogenation of CO_2 on group VIII metals: II. Kinetics and mechanism of CO_2 hydrogenation on nickel. *J. Catal.* **1982**, *77*, 460−472.

(10) Marwood, M.; Doepper, R.; Renken, A. In-situ surface and gas phase analysis for kinetic studies under transient conditions The catalytic hydrogenation of CO_2. *Appl. Catal. A* **1997**, *151*, 223−246.

(11) Schild, C.; Wokaun, A.; Baiker, A. On the mechanism of CO and CO_2 hydrogenation reactions on zirconia-supported catalysts: a diffuse reflectance FTIR study: Part II. Surface species on copper/zirconia catalysts: implications for methanoi synthesis selectivity. *J. Mol. Catal.* **1990**, *63*, 243−254.

(12) Lin, W.; Stocker, K. M.; Schatz, G. C. Mechanisms of Hydrogen-Assisted CO_2 Reduction on Nickel. *J. Am. Chem. Soc.* **2017**, *139*, 4663−4666.

(13) Vesselli, E.; Rizzi, M.; De Rogatis, L.; Ding, X.; Baraldi, A.; Comelli, G.; Savio, L.; Vattuone, L.; Rocca, M.; Fornasiero, P.; Baldereschi, A.; Peressi, M. Hydrogen-Assisted Transformation of CO_2 on Nickel: The Role of Formate and Carbon Monoxide. *J. Phys. Chem. Lett.* **2010**, *1*, 402−406.

(14) Vesselli, E.; De Rogatis, L.; Ding, X.; Baraldi, A.; Savio, L.; Vattuone, L.; Rocca, M.; Fornasiero, P.; Peressi, M.; Baldereschi, A.; Rosei, R.; Comelli, G. Carbon Dioxide Hydrogenation on Ni(110). *J. Am. Chem. Soc.* **2008**, *130*, 11417−11422.

(15) Fujita, S.-I.; Usui, M.; Takezawa, N. Mechanism of the reverse water gas shift reaction over Cu/ZnO catalyst. *J. Catal.* **1992**, *134*, 220−225.

(16) Dietz, L.; Piccinin, S.; Maestri, M. Mechanistic Insights into CO_2 Activation via Reverse Water−Gas Shift on Metal Surfaces. *J. Phys. Chem. C* **2015**, *119*, 4959−4966.

(17) Wang, L. C.; Tahvildar Khazaneh, M.; Widmann, D.; Behm, R. J. TAP reactor studies of the oxidizing capability of CO_2 on a Au/CeO_2 catalyst − A first step toward identifying a redox mechanism in the Reverse Water−Gas Shift reaction. *J. Catal.* **2013**, *302*, 20−30.

(18) Heine, C.; Lechner, B. A. J.; Bluhm, H.; Salmeron, M. Recycling of CO_2: Probing the Chemical State of the Ni(111) Surface during the Methanation Reaction with Ambient-Pressure X-Ray Photoelectron Spectroscopy. *J. Am. Chem. Soc.* **2016**, *138*, 13246−13252.
(19) Cai, J.; Han, Y.; Chen, S.; Crumlin, E. J.; Yang, B.; Li, Y.; Liu, Z. CO_2 Activation on Ni(111) and Ni(100) Surfaces in the Presence of H_2O: An Ambient-Pressure X-ray Photoelectron Spectroscopy Study. *J. Phys. Chem. C* **2019**, *123*, 12176−12182.
(20) Ledentu, V.; Dong, W.; Sautet, P. Heterogeneous Catalysis through Subsurface Sites. *J. Am. Chem. Soc.* **2000**, *122*, 1796−1801.
(21) Bhatia, B.; Sholl, D. S. Chemisorption and diffusion of hydrogen on surface and subsurface sites of flat and stepped nickel surfaces. *J. Chem. Phys.* **2005**, *122*, 204707.
(22) Ceyer, S. T. The Unique Chemistry of Hydrogen beneath the Surface: Catalytic Hydrogenation of Hydrocarbons. *Acc. Chem. Res.* **2001**, *34*, 737−744.
(23) Ghosh, A.; Hsu, B. B.; Dougal, S. M.; Afeworki, M.; Stevens, P. A.; Yeganeh, M. S. Effects of Gas Feed Ratios and Sequence on Ethylene Hydrogenation on Powder Pt Catalyst Studied by Sum Frequency Generation and Mass Spectrometry. *ACS Catal.* **2014**, *4*, 1964−1971.
(24) Vesselli, E.; Schweicher, J.; Bundhoo, A.; Frennet, A.; Kruse, N. Catalytic CO_2 Hydrogenation on Nickel: Novel Insight by Chemical Transient Kinetics. *J. Phys. Chem. C* **2011**, *115*, 1255−1260.
(25) Salmeron, M.; Schlögl, R. Ambient pressure photoelectron spectroscopy: A new tool for surface science and nanotechnology. *Surf. Sci. Rep.* **2008**, *63*, 169−199.
(26) Toyoshima, R.; Yoshida, M.; Monya, Y.; Kousa, Y.; Suzuki, K.; Abe, H.; Mun, B. S.; Mase, K.; Amemiya, K.; Kondoh, H. In Situ Ambient Pressure XPS Study of CO Oxidation Reaction on Pd(111) Surfaces. *J. Phys. Chem. C* **2012**, *116*, 18691−18697.
(27) Toyoshima, R.; Yoshida, M.; Monya, Y.; Suzuki, K.; Amemiya, K.; Mase, K.; Mun, B. S.; Kondoh, H. A high-pressure-induced dense CO overlayer on a Pt(111) surface: a chemical analysis using in situ near ambient pressure XPS. *Phys. Chem. Chem. Phys.* **2014**, *16*, 23564−23567.
(28) Hao, X.; Wang, B.; Wang, Q.; Zhang, R.; Li, D. Insight into both coverage and surface structure dependent CO adsorption and activation on different Ni surfaces from DFT and atomistic thermodynamics. *Phys. Chem. Chem. Phys.* **2016**, *18*, 17606−17618.
(29) Grass, M. E.; Karlsson, P. G.; Aksoy, F.; Lundqvist, M.; Wannberg, B.; Mun, B. S.; Hussain, Z.; Liu, Z. New ambient pressure photoemission endstation at Advanced Light Source beamline 9.3.2. *Rev. Sci. Instrum.* **2010**, *81*, No. 053106.
(30) Chang, R.; Hong, Y. P.; Axnanda, S.; Mao, B.; Jabeen, N.; Wang, S.; Tai, R.; Liu, Z. In-situ photoelectron spectroscopy with online activity measurement for catalysis research. *Curr. Appl. Phys.* **2012**, *12*, 1292−1296.
(31) Hamza, A. V.; Madix, R. J. Dynamics of the dissociative adsorption of hydrogen on nickel(100). *J. Phys. Chem.* **1985**, *89*, 5381−5386.
(32) Panczyk, T.; Szabelski, P.; Rudzinski, W. Hydrogen Adsorption on Nickel (100) Single-Crystal Face. A Monte Carlo Study of the Equilibrium and Kinetics. *J. Phys. Chem. B* **2005**, *109*, 10986−10994.
(33) Christmann, K.; Schober, O.; Ertl, G.; Neumann, M. Adsorption of hydrogen on nickel single crystal surfaces. *J. Chem. Phys.* **1974**, *60*, 4528−4540.
(34) Behm, R. J.; Brundle, C. R. On the formation and bonding of a surface carbonate on Ni(100). *Surf. Sci.* **1991**, *255*, 327−343.
(35) He, H.; Okawa, Y.; Tanaka, K.-I. Hydrogenation of carbidic carbon on the Ni(100) surface. *Surf. Sci.* **1997**, *376*, 310−318.
(36) Goodwan, D. W.; Kelley, R. D.; Madey, T. E.; White, J. M. Measurement of carbide buildup and removal kinetics on Ni(100). *J. Catal.* **1980**, *64*, 479−481.
(37) Wang, Z.; Cao, X. M.; Zhu, J.; Hu, P. Activity and coke formation of nickel and nickel carbide in dry reforming: A deactivation scheme from density functional theory. *J. Catal.* **2014**, *311*, 469−480.
(38) Liu, J.-X.; Zhang, B.-Y.; Chen, P.-P.; Su, H.-Y.; Li, W.-X. CO Dissociation on Face-Centered Cubic and Hexagonal Close-Packed Nickel Catalysts: A First-Principles Study. *J. Phys. Chem. C* **2016**, *120*, 24895−24903.
(39) Wu, C. H.; Eren, B.; Bluhm, H.; Salmeron, M. B. Ambient-Pressure X-ray Photoelectron Spectroscopy Study of Cobalt Foil Model Catalyst under CO, H_2, and Their Mixtures. *ACS Catal.* **2017**, *7*, 1150−1157.
(40) Sehested, J.; Dahl, S.; Jacobsen, J.; Rostrup-Nielsen, J. R. Methanation of CO over Nickel: Mechanism and Kinetics at High H_2/CO Ratios. *J. Phys. Chem. B* **2005**, *109*, 2432−2438.
(41) Hanlon, J. F. *A User's Guide to Vacuum Technology*, 3rd ed.; John Wiley & Sons, Inc.: Hoboken, NJ, 2003
(42) Wang, S.-G.; Cao, D.-B.; Li, Y.-W.; Wang, J.; Jiao, H. Chemisorption of CO_2 on Nickel Surfaces. *J. Phys. Chem. B* **2005**, *109*, 18956−18963.
(43) Benziger, J. B.; Madix, R. J. The decomposition of formic acid on Ni(100). *Surf. Sci.* **1979**, *79*, 394−412.
(44) Snoeck, J. W.; Froment, G. F.; Fowles, M. Steam/CO_2 Reforming of Methane. Carbon Filament Formation by the Boudouard Reaction and Gasification by CO_2, by H_2, and by Steam: Kinetic Study. *Ind. Eng. Chem. Res.* **2002**, *41*, 4252−4265.
(45) Kaiser, P.; Unde, R. B.; Kern, C.; Jess, A. Production of Liquid Hydrocarbons with CO_2 as Carbon Source based on Reverse Water-Gas Shift and Fischer-Tropsch Synthesis. *Chem. Ing. Tech.* **2013**, *85*, 489−499.
(46) Peebles, D. E.; Goodman, D. W.; White, J. M. Methanation of carbon dioxide on nickel(100) and the effects of surface modifiers. *J. Phys. Chem.* **1983**, *87*, 4378−4387.

https://doi.org/10.1021/acscatal.3c01517
ACS Catal. 2023, 13, 9041−9050